ACADEMIA ROMÂNĂ
Revue Roumaine de Chimie
https://www.icf.ro/rrch/

Rev. Roum. Chim.,
2024, *69*(1–2), 19–24
DOI: 10.33224/rrch.2024.69.1-2.02

ENHANCED PHOTOCATALYTIC ACTIVITY OF COPPER-DOPED ZnO NANOCRYSTALS SYNTHESIZED BY A HYDROTHERMAL ROUTE

Zaineb HAMMAMI,[a] Bilel CHOUCHENE,[b] Mouldi ZOUAOUI,[c] Tahar BEN CHAABANE[a*] and Raphaël SCHNEIDER[b]

[a]University of Carthage, Faculty of Sciences of Bizerte, LR 18 ES11 Laboratory of hetero-organic compounds and nanostructured materials, 7021 Jarzouna, Bizerte, Tunisia
[b]University of Lorraine, CNRS, LRGP, F-54000 Nancy, France
[c]University of Carthage, Faculty of Sciences of Bizerte, LR01ES15 Bizerte, Tunisia

Received January 30, 2023

$Zn_{(1-x)}Cu_xO$ (x = 0, 1, 3, 5%) nanocrystals were synthesized via a hydrothermal method at 150°C for 24 h. The structural, morphological, optical and photocatalytic properties of the samples were investigated, and found to be dependent on the content of the copper dopant. The UV photocatalytic activities of $Zn_{(1-x)}Cu_xO$ nanocrystals were evaluated by the photodecomposition of the methyl orange (MO) dye. The nanocrystals with a Cu content of 5% exhibited the highest UV photocatalytic activity with a photodegradation efficiency of 94% during 120 min as compared to that of pure ZnO with 73%. The enhancement of the photocatalytic activity of $Zn_{0.95}Cu_{0.05}O$ originates from the better separation of the photogenerated electron-hole pairs.

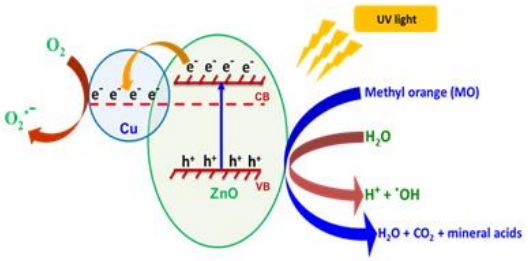

INTRODUCTION

Owing to its interesting physicochemical properties, zinc oxide ZnO remains among the most studied materials in fundamental and applied research. ZnO is an attractive material because of its multiple applications in various fields.[1–3] For instance, pure and doped ZnO present interesting photocatalytic activities to degrade organic colorants in an aqueous solution.[4,5] The application of various dyes in textiles, leather, paper, ..., generates considerable quantities of environmentally hazardous effluents. ZnO, whether pure or doped, can be used to find solutions for wastewater decontamination. Doping ZnO with a given metal (Mn, Cu, Co,...) can significantly promote its photocatalytic efficiency. ZnO-Cu nanocrystals often show an improvement in the photocatalytic capacity as compared to pure ZnO.[6–8] The present work deals with the effect of the Cu doping on the UV photocatalytic activity of ZnO to decompose the anionic methyl orange (MO) dye taken as a model pollutant. We report the hydrothermal synthesis of $Zn_{(1-x)}Cu_xO$ (x = 0, 1, 3, 5%) nanocrystals, the investigation of their structural,

* Corresponding author: taharbch@yahoo.com

morphological, optical, and photocatalytic characteristics.

EXPERIMENTAL

1. Materials and samples preparation

Zinc chloride ($ZnCl_2$, Fluka, 98%), copper chloride ($CuCl_2$, Fluka, 98%), polyvinylpyrrolidone (PVP K30, Sigma-Aldrich) as a dispersing agent, and sodium hydroxide (NaOH, Sigma Aldrich, 98%) were used to prepare $Zn_{(1-x)}Cu_xO$ samples. All nanocrystals were prepared by a hydrothermal method using twice-distilled water. Typically, PVP K30 (1667 mg), NaOH (360 mg, 0.2M), and zinc chloride (409 mg, 0.2 M) were mixed in 15 mL of twice-distilled water (solution S1). The mixture was maintained under vigorous stirring for 20 min, then transferred in a 20 mL Teflon-sealed autoclave and was heated at 150 °C in an electrical oven for 24 h. The ZnO nanocrystals were collected by centrifugation, washed several times with water and ethanol, then air-dried at 60 °C for 12 h. For Cu^{2+}-doped zinc oxide ($Zn_{(1-x)}Cu_xO$) with different copper content x = 0, 1, 3, and 5 at %, the appropriate amount of $CuCl_2$ was added to the solution S1 subjected to the same procedure as before. In the following, $Zn_{(1-x)}Cu_xO$ is labeled as ZCu(x) for a particular value of x and the overall series $Zn_{(1-x)}Cu_xO$ are denoted ZCu.

2. Photocatalytic experiments

The photocatalytic degradation of MO (Biochem, 98%) was conducted under UV light irradiation produced by two Actinic BL TL 8W mercury lamps emitting around 370 nm. A typical reaction involves the dispersion of 60 mg of the catalyst in 60 mL of methyl orange (MO) solution (10 $mg \cdot L^{-1}$) at a controlled neutral pH and keeping it under continual stirring for 50 min in the dark to reach the adsorption/desorption equilibrium. Next, the light was turned on. At equal intervals of irradiation time (20 min), 2 mL of the reaction solution was taken out, and centrifuged (12,000 rpm for 3 min) to remove the photocatalyst. The UV–Visible spectra of the supernatants were recorded with a Perkin Elmer apparatus.

3. Characterization

The XRD data were collected in 2θ range: 5°–70° using an X'Pert MPD diffractometer operating with Cu (Kα) radiation (λ = 1.5418 Å). Transmission electron microscopy (TEM) images were taken by using a Tecnai G2 TEM operating at 200 kV. Energy Dispersive X-Ray Analysis (EDX) where performed using JSM-6490 LV equipment. The diffuse reflectance spectra were obtained using a Shimadzu 2600 UV–visible spectrophotometer in the interval 300–800 nm.

RESULTS AND DISCUSSION

1. Structural and micro-structural analysis

The X-ray diffraction (XRD) patterns of the prepared ZCu powders are displayed in Fig. 1. All the patterns exhibit diffraction peaks of the ZnO wurtzite phase (JCPDS file N° 36-1451).[9]

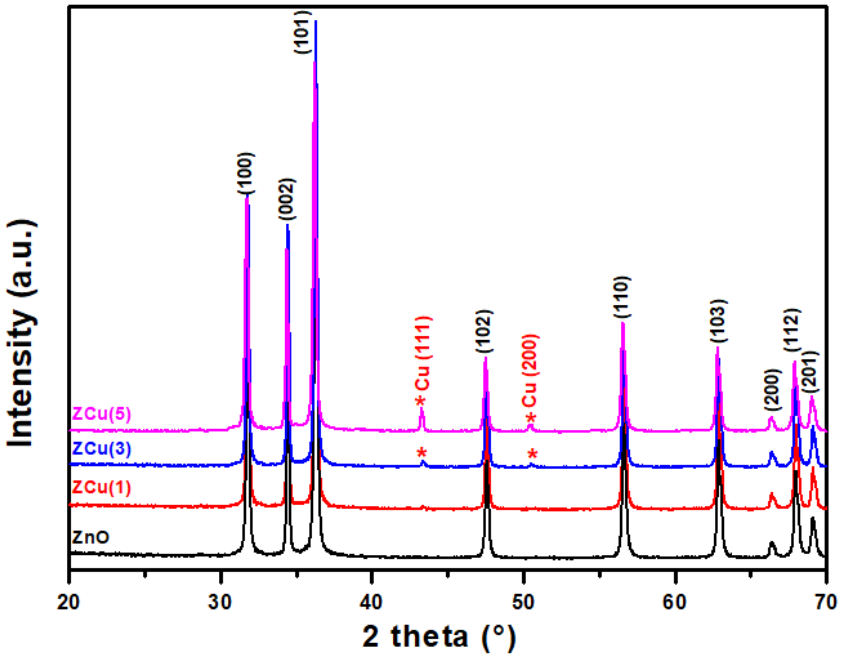

Fig. 1 – XRD patterns of ZCu (0, 1, 3, 5%) nanocrystals.

For ZCu (3 and, 5 %) samples, minor additional peaks at 2θ values of 43.39 and 50.55° corresponding to the cubic phase of metallic Cu could be observed (space group Fm-3m),[10] and

their intensity increases with the Cu content. Figure 2 displays the TEM images of ZnO, ZCu(3), and ZCu(5) samples and shows the presence of irregularly shaped platelets with sizes varying between 200 and 300 nm. Some rod-like shapes whose size and abundance depend on the Cu dopant concentration are also observed. For pure ZnO, these rods are only a very minor fraction of the sample and of low size (150–250 nm in length and about 60 nm in diameter) (Fig. 2a). For the ZCu(3) sample, the rod sizes increase slightly both in length (160–350 nm) and in diameter (60–70 nm). For the ZCu(5) sample, larger rods with lengths up to 400-500 nm and diameters up to 60–80 nm were formed (Fig. 2c).

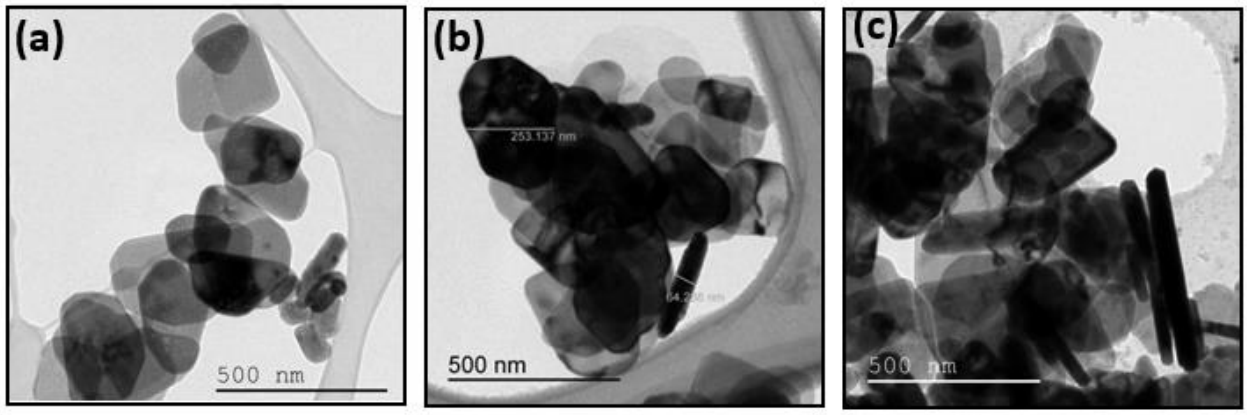

Fig. 2 – TEM images of (a) pure ZnO, (b) ZCu(3), and (c) ZCu (5).

Table 1 displays the sample's nominal Cu/Zn ratios and the actual ones as determined by energy dispersive X-ray spectroscopy. It reveals that Cu was present in all doped ZnO nanostructures and the measured ratios Cu/Zn increased with copper content.

Table 1

Gap energies, nominal Cu/Zn ratios, and actual ones as obtained from EDX analysis of ZCu samples

Sample	**ZnO**	**ZCu(1)**	**ZCu(3)**	**ZCu(5)**
Gap E_g (eV)	3.21	3.19	3.20	3.19
Actual Cu/Zn	–	0.013	0.047	0.056
Nominal Cu/Zn	–	0.010	0,031	0,053

For ZCu(1) and ZCu(5) particles, the actual Cu/Zn ratios were very close to those of the starting precursors. A positive deviation of the actual Cu/Zn ratio is observed for ZCu(3) nanocrystals that suggests some zinc deficiency for this sample.

2. Optical properties

Fig. 3a shows the UV-visible absorption spectra of ZCu particles. A significant increase in absorption for all nanocrystals can be observed towards 377 nm, a value in accordance with the optical bandgap of ZnO.[11] In the visible range (400–750 nm), ZnO and ZCu(1) nanocrystals only weakly absorb while a slightly increased absorption is observed for ZCu(3) and ZCu(5) samples. The optical bandgaps E_g of the samples were determined by plotting the Tauc's curves[12] from the equation (1):

$$(\alpha h\nu)^2 = A\,(h\nu - E_g) \qquad (1)$$

where α, A, h, and ν are the absorption coefficient, a constant, Planck constant, and photon frequency, respectively. The Tauc's plots representing $(\alpha h\nu)^2$ *versus* $h\nu$ are shown in Fig. 3b; the obtained bandgaps values were almost similar, varying between 3.21 and 3.19 eV, which indicated that the sample's bandgaps were not significantly affected by the Cu doping (Table 1).

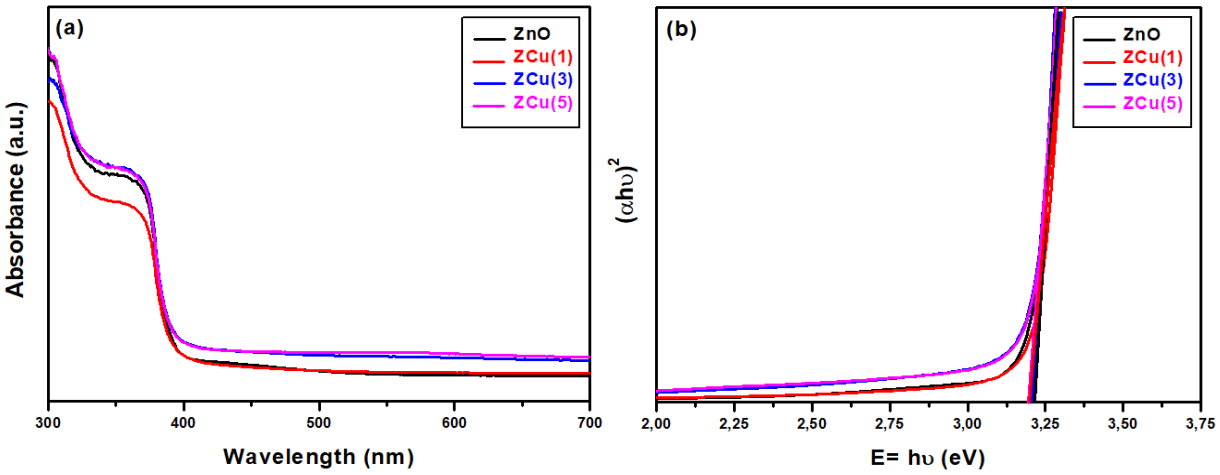

Fig. 3 – a) UV-visible absorbance spectra for ZCu (0, 1, 3, 5 %) nanocrystals and b) the corresponding Tauc's plots.

3. Photocatalytic activity of ZCu catalysts

Figure 4 shows the UV-visible absorption spectra of MO during photocatalytic tests using ZnO and ZCu (5) samples.

Note the progressive decrease of the absorbance of MO at 464 and at 271 nm for both catalysts, which indicates that the OM degradation takes place. The latter signal (271 nm) is characteristic of phenyl groups and the former one (464 nm) can be assigned to azo groups (–N=N–)[13] (Fig. 4).

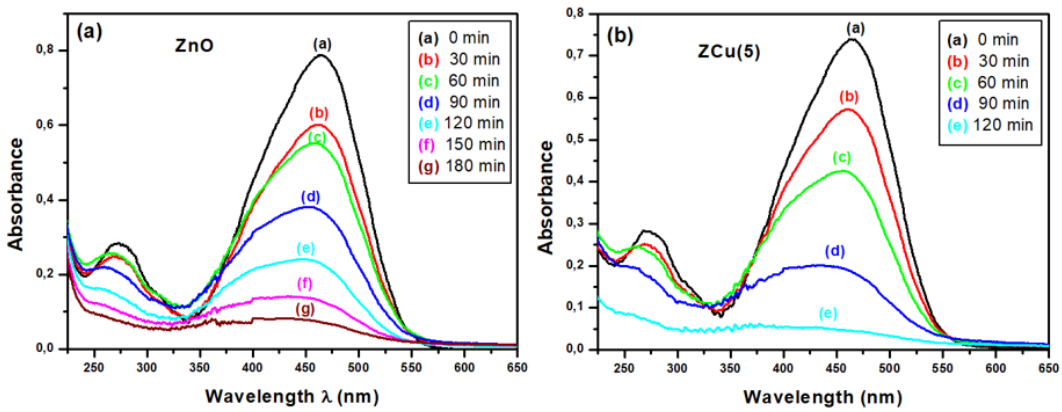

Fig. 4 – UV-visible absorbance spectra of MO as a function of irradiation time for a) ZnO and b) ZCu(5) catalysts.

The photodegradation efficiency (PE) for MO was calculated as:

$$PE = [(C_0 - C_t)/C_0]\cdot 100\ \% \qquad (2)$$

where C_0 and C_t are the concentrations of MO at t = 0 and at the time t of the irradiation, respectively. The PE values for ZCu catalysts, determined at 120 min of irradiation, are displayed in Table 2. The highest PE value (94%) corresponds to the ZCu(5) catalysts.

Table 2

Kinetic order and photodegradation efficiency of MO for ZCu series

Sample	Zero-order kinetic k_0 (mg·L^{-1}·min^{-1});	*R^2 (%)	First order kinetic k_1 (min^{-1});	*R^2(%)	Photodegradation efficiency (PE %) at 120min
ZnO	59.87×10^{-3};	**98.66**	13.69×10^{-3};	92.31	73
ZCu (1)	52.05×10^{-3};	**99.33**	13.53×10^{-3};	94.71	70
ZCu (3)	44.20×10^{-3};	**95.94**	9.66×10^{-3};	87.98	46
ZCu (5)	77.11×10^{-3};	**99.44**	22.41×10^{-3};	88.20	94

*R^2 refers to the correlation coefficient.

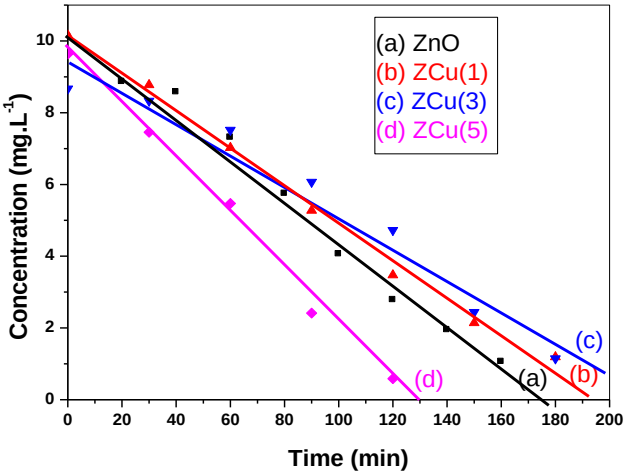

Fig. 5 – Zero-order rate plots of the MO photodegradation for ZCu photocatalysts.

We examined the validity of the zero-order and the pseudo-first order kinetics that take respectively the following forms: $C_t = -k_0 t + C_0$ and $\ln(C_0/C_t) = k_1 t$, where k_0 and k_1 refer to the corresponding rate constants. The values of k_0 and k_1 were determined from the slopes of the linear fits for zero and first order, respectively, and are given in Table 2. The highest R^2 values ranging from 95.94 to 99.44% match well with zero order kinetic[14,15] that was illustrated in Fig. 5. As expected, the maximal constant k_0 of 77.11×10^{-3} mg·L^{-1}·min^{-1} is obtained for the ZCu (5) catalyst with the optimal Cu content.

4. Photodegradation mechanism using ZCu catalysts

To investigate the main photogenerated species involved in the MO photodegradation process, some experiments using the ZCu(5) catalyst in the presence of scavengers were carried out.

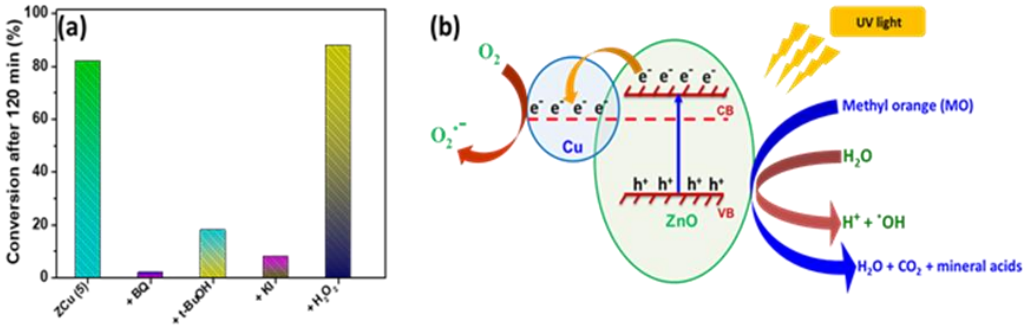

Fig. 6 – a) UV photodegradation efficiency of MO using the ZCu (5) catalyst with and without scavengers, b) schematic illustration of the proposed photocatalytic mechanism for the MO photodegradation.

When benzoquinone (10^{-3} M), t-BuOH (40 mL/L), or KI (10^{-2} M), respectively used as scavengers of $O_2^{\bullet-}$ and $^{\bullet}OH$ radicals and of holes (h^+)[16,17] were added to the dye solution, the degradations were strongly reduced (Fig. 6a). Hydrogen peroxide H_2O_2 (0.19 M), used as electron scavenger, had no significant effect indicating that the major part of the electrons reacts with O_2 to generate $O_2^{\bullet-}$ radicals. It can be concluded that $O_2^{\bullet-}$ and $^{\bullet}OH$ radicals and h^+ are the main active species involved in the MO decomposition.[11,18] Based on these results, a plausible photocatalytic mechanism can be proposed. As schematically illustrated in Fig. 6b, following the UV excitation of the photocatalyst, electrons e^- are transferred from the valence band (VB) to the conduction band (CB) of ZnO, leaving holes h^+ in the VB. Due to the close contact of ZnO and Cu particles, a Schottky barrier is created at the interface. Then, the Fermi levels of ZnO and Cu particles combine to generate a new equilibrium state Fermi level. Thus, the photogenerated electrons can be transferred to Cu particles that act as electron sinks. Next, these electrons react with adsorbed O_2 molecules to

produce $O_2^{\bullet-}$ radicals. The holes (h^+) remaining in the VB react with OH^- or with H_2O to produce ($^{\bullet}OH$) radicals. Holes can also directly oxidize MO into MO^+. The photoproduced $O_2^{\bullet-}$, h^+, and $^{\bullet}OH$ species are responsible for MO decomposition into CO_2, H_2O, and degradation products.

CONCLUSION

Cu-doped zinc oxide $Zn_{(1-x)}Cu_xO$ (x = 0, 1, 3, and 5 %) nanocrystals were synthesized using a simple and cost-effective hydrothermal method. The photocatalytic activity of the 5% Cu-doped ZnO under UV irradiation is higher than that of pure ZnO with a PE of 94% after 120 min irradiation. The optimal Cu doping of 5% provides the best separation efficiency of the photogenerated carrier charges. Therefore, ZCu (5) nanocrystals have proven to be an effective way to clean up wastewater contaminated by different dyes.

REFERENCES

1. G. Dubourg, M. Radovi´c and B. Vasi´c, *Nanomater.* **2021**, *11*, 1–11.
2. I. Constantinoiu and C. Viespe, *Sensors*, **2020**, *20*, 1–20.
3. Z. Mirzaeifard, Z. Shariatinia, M. Jourshabani and S. M. Rezaei Darvishi, *Ind. Eng. Chem. Res.*, **2020**, *59*, 15894–15911
4. S. M. EL-Dafrawy, M. Tarek, S. Samra and S. M. Hassan, *Sci. Rep.*, **2021,** *11*, 11404–11411.
5. M. Pavithra and M. B. Jessie Raj, *Ceram. Intern.*, **2021**, *47*, 32324–32331.
6. F. P. Delgado, L. A. Hermida-Montero, J. E. Morales-Mendoza, Z. Dur´an-Barradas, A. I. Mtz-Enriquezc and N. Pariona, *RSC Adv.*, **2022,** *12*, 9898–9908.
7. M. Rabbani, J. Shokraiyan, R. Rahimi and R. Amrollahi, *Water Sci.Tech.*, **2021**, *84*, 1813–1825.
8. L. Pandian , R. Rajasekaran and P. Govindan, *Mater. Res. Express*, **2018**, *5*, 115505–115511.
9. F. Xu, P. Zhang, A. Navrotsky, Z.-Y. Yuan, T.-Z. Ren, M. Halasa and B.-L. Su, *Chem. Mater.*, **2007**, *19*, *5680–5686.*
10. H. R. Khan, G. Murtaza, M. A. Choudhary, Z. Ahmed and M. A. Malik, *Sol. Energy.*, **2018**, *173*, 875–881.
11. N. A. Putri, V. Fauzia, S. Iwan, L. Roza, A. A. Umar and S. Budi, *Appl. Surf. Sci.*, **2018**, *439*, 285–297.
12. R. Ahmad Zargar, *Sci. Rep.*, **2022,** *12*, 1–10.
13. N. Panda, H. Sahoo and S. Mohapatra, *J. Hazard. Mater*., **2011**, *185*, 359–365.
14. S. Khezrianjoo, J. Lee, K.-H. Kim and V. Kumar, *Catalysts*., **2019**, *9*, 871–878.
15. U. I. Gaya, A. H. Abdullah, Z. Zainal and M. Z. Hussein, *J. Hazard. Mater*., **2009**, *168*, 57–63.
16. A. T. Zajac, M. Synowiec, K. Zakrzewska, K. Zazakowny, K. Kowalski, A.Dziedzic and M. Radecka, *ACS Appl. Mater. Interf.*, **2022**, *14*, 38255−38269.
17. X. Chen, Z. Wu, D. Liu and Z. Gao, *Nanoscale Res Lett*., **2017**, *12*, 143.
18. S. Kuriakose, B. Satpati and S. Mohapatra, *Phys. Chem. Chem. Phys*., **2014,** *16*, 12741–12749.